

# A boundary element method for the analysis of CNT/polymer composites with a cohesive interface model based on molecular dynamics

Y.J. Liu<sup>a,\*</sup>, N. Nishimura<sup>b</sup>, D. Qian<sup>a</sup>, N. Adachi<sup>b</sup>, Y. Otani<sup>b</sup>, V. Mokashi<sup>a</sup>

<sup>a</sup>Department of Mechanical, Industrial and Nuclear Engineering, University of Cincinnati, P.O. Box 210072, Cincinnati, OH 45221-0072, USA

<sup>b</sup>Academic Center for Computing and Media Studies, Kyoto University, Kyoto 606-8501, Japan

Received 6 January 2006; accepted 11 November 2007

Available online 2 January 2008

## Abstract

In this paper, a new cohesive interface model is applied to characterize carbon nanotube (CNT) composites using the boundary element method (BEM). In the previous BEM models of CNT composites, a rigid-inclusion model was employed to represent the CNTs in a polymer matrix due to their extremely high stiffness as compared with the polymer. Perfect bonding interface conditions between the CNT fibers and matrix were used in these earlier models. Very good BEM results for the effective moduli were obtained as compared with other multi-scale models based on molecular dynamics (MD) and continuum mechanics. However, these simulation results yield much higher estimates of the effective Young's moduli of CNT/polymer composites than those observed in experiments of such composites. This discrepancy is largely due to the interfaces in CNT composites which have been found to be weakly, rather than strongly bonded. In this work, a new cohesive interface model has been developed by using MD simulations and employed in the BEM models to replace the perfect bonding interface models. The parameters in the cohesive interface model are obtained by conducting CNT pull-out simulations with MD and these parameters are subsequently used in the BEM models of the CNT/polymer composites. Marked decreases of the estimated effective Young's moduli are observed using the new BEM models with the cohesive interface conditions. The developed BEM models combined with the MD can be a very useful tool for studying the interface effects in CNT composites and for large-scale characterizations of such nanocomposites.

© 2007 Elsevier Ltd. All rights reserved.

**Keywords:** Carbon nanotube composites; Cohesive interface models; Boundary element method; Multi-scale modeling; Large-scale modeling

## 1. Introduction

Carbon nanotubes (CNT) have been found to have very high elastic moduli along their axial directions, with an averaged value around 1 TPa, which are ideal for making a new class of nanocomposites [1–9]. To characterize these CNT composites using computational methods in order to extract their effective mechanical properties, various approaches have been proposed in recent years, including molecular dynamics [10], continuum mechanics with finite element method (FEM) and boundary element method (BEM) [11–16], and multi-scale approaches combining MD

and continuum models [17,18]. However, these simulation results in general yield overestimated properties of the CNT composites, such as higher effective Young's moduli, than those observed in experiments [1,19–21]. This may be due to the fact that in these simulation models, idealized conditions are often assumed, especially the perfect bonding conditions at the interfaces between the CNTs and matrix.

Interface is one of the key factors for load transfer in CNT composites, besides alignment and dispersion of the CNTs in a matrix. It is observed in experiments that the load transfer mechanism in CNT composites is weak due to the difficulties in making strong bond between CNT fibers and polymer matrix [1,19–21]. CNTs often interact with the molecules of the polymer matrix through mainly van der

\*Corresponding author. Tel.: +1 513 556 4607.

E-mail address: [Yijun.Liu@uc.edu](mailto:Yijun.Liu@uc.edu) (Y.J. Liu).

Waals forces. Therefore, perfect bonding or any other strong bond interface conditions in various MD or continuum models of CNT composites will result in overestimated effective stiffness for the composites. New interface models, that can account for the weak interactions between CNTs and their host matrix, need to be developed. In addition, large-scale models that can account for random alignment and dispersions of the CNT fibers in a matrix are also needed. These improved models of the CNT composites will improve the correlation of the simulation results with the experimental ones. The improved interface models can also be employed to study the effects of different interface parameters and hence help to design better CNT composites.

Continuum models have been found to be very close to MD models and thus adequate for studying the overall mechanical properties of the CNT composites (see, e.g., Refs. [10,22]). Among the continuum models, the FEM and BEM approaches have been applied. A fast multipole BEM for large-scale modeling of CNT composites using a rigid-inclusion approach was developed recently [16]. In this BEM approach to modeling CNT composites, a rigid-inclusion model was employed to represent the CNTs in an elastic polymer matrix due to the high stiffness of the CNTs. The perfect bonding conditions between the CNT fibers and matrix were used in these BEM models. Very large 3-D representative volume elements (RVEs) containing up to 16,000 CNT fibers and with the total DOFs above 28 millions were successfully solved by using this fast multipole BEM. Although the rigid-inclusion model may be sufficient for modeling the CNTs, the perfect bonding conditions for the interfaces may not be adequate. In this paper, a new cohesive interface model is presented to improve the BEM models in Ref. [16] for modeling CNT composites. This cohesive interface model is developed with the help of MD simulations of CNT pull-outs from a polymer matrix under several load conditions. Numerical results show that the cohesive interface model has a significant impact to the estimated effective Young's moduli of the CNT/polymer composites. Lower effective Young's moduli are obtained with the new interface model, as compared with those based on perfect bonding conditions. These new results are closer to those observed in experiments and believed to be more realistic.

This paper is organized as follows: In Section 2, the boundary integral equation (BIE) formulation and the new cohesive interface model are presented. In Section 3, the ways to determine the parameters in the cohesive interface model using the MD simulations are described. In Section 4, numerical results are presented to show the effects of the new interface model. Sections 5 and 6 are discussions and conclusions, respectively, to conclude this paper.

## 2. The boundary integral equation formulation

We first develop the BIE formulation for the problem and then discuss the interface conditions to be employed

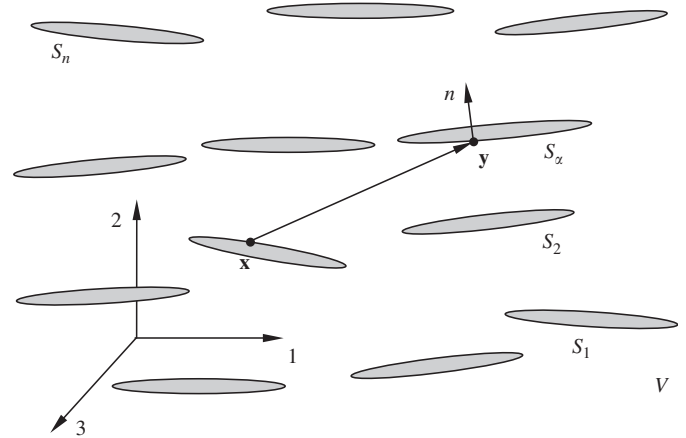


Fig. 1. A 3-D infinite elastic domain  $V$  embedded with rigid inclusions.

for this study. Consider a 3-D infinite elastic domain  $V$  embedded with  $n$  CNTs (or rigid inclusions, Fig. 1). The domain  $V$  is loaded with a remote stress or displacement field. The BIE for this problem in domain  $V$  can be written as (see, e.g., Refs. [23–25]):

$$\frac{1}{2} \mathbf{u}(\mathbf{x}) = \int_S [\mathbf{U}(\mathbf{x}, \mathbf{y}) \mathbf{t}(\mathbf{y}) - \mathbf{T}(\mathbf{x}, \mathbf{y}) \mathbf{u}(\mathbf{y})] dS(\mathbf{y}) + \mathbf{u}^\infty(\mathbf{x}), \quad \forall \mathbf{x} \in S, \quad (1)$$

where  $\mathbf{u}$  and  $\mathbf{t}$  are the displacement and traction vectors, respectively;  $S = \cup S_\alpha$  with  $S_\alpha$  being the boundary (assumed to be smooth) of the  $\alpha$ th inclusion (Fig. 1); and  $\mathbf{u}^\infty$  the undisturbed displacement field due to the remote stress or displacement field. For a finite (interior) domain, this term will not present in Eq. (1). The two kernel functions  $\mathbf{U}(\mathbf{x}, \mathbf{y})$  and  $\mathbf{T}(\mathbf{x}, \mathbf{y})$  in Eq. (1) are the displacement and traction components of the fundamental solution (Kelvin's solution), respectively, which can be found in any references on the BEM (e.g., Refs. [23–25]). All the variables in BIE (1) are associated with the matrix domain  $V$ .

If we assume that the CNTs can be modeled as rigid inclusions, then the displacement at any point  $\mathbf{y}$  on the CNT enclosed by  $S_\alpha$  can be described by rigid-body motions as follows:

$$\mathbf{u}^{(CNT)}(\mathbf{y}) = \mathbf{d} + \boldsymbol{\omega} \times \mathbf{p}(\mathbf{y}), \quad (2)$$

where  $\mathbf{d}$  is the rigid-body translational displacement vector,  $\boldsymbol{\omega}$  the rotation vector and  $\mathbf{p}$  a position vector for point  $\mathbf{y}$  measured from a reference point (such as the center of the CNT).

We now propose an interface model for the cohesive interfaces between the CNTs and matrix (Fig. 2). In this cohesive interface model, the difference of the displacement fields  $\mathbf{u}^{(CNT)}$  in the CNT and  $\mathbf{u}$  in the matrix is related to the traction  $\mathbf{t}$  at the interface (from the matrix domain) in the following form:

$$\mathbf{u}^{(CNT)}(\mathbf{y}) - \mathbf{u}(\mathbf{y}) = \mathbf{C}(\mathbf{y}) \mathbf{t}(\mathbf{y}), \quad \forall \mathbf{y} \in S_\alpha, \quad (3)$$

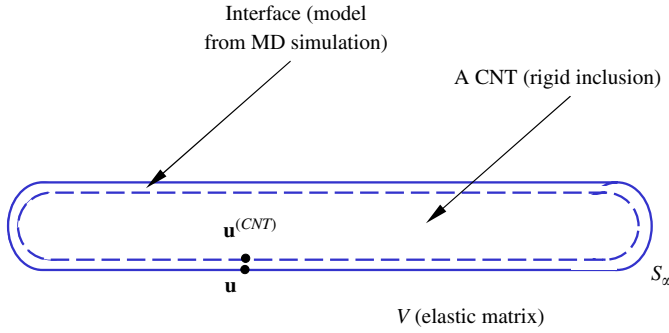


Fig. 2. The interface between the CNT (rigid inclusion) and matrix.

where  $\mathbf{C}$  is a “compliance” matrix to be determined by the MD simulations (see Section 3).

Considering the BIE for the rigid inclusion (CNT) itself in the domain enclosed by  $S_z$  and the equilibrium of the tractions at the interface, and using the interface condition given in Eq. (3), it can be shown that BIE (1) is reduced to

$$\begin{aligned} & \mathbf{u}^{(CNT)}(\mathbf{x}) - \frac{1}{2}\mathbf{C}(\mathbf{x})\mathbf{t}(\mathbf{x}) \\ &= \int_S [\mathbf{U}(\mathbf{x}, \mathbf{y}) + \mathbf{T}(\mathbf{x}, \mathbf{y})\mathbf{C}(\mathbf{y})]\mathbf{t}(\mathbf{y}) dS(\mathbf{y}) \\ &+ \mathbf{u}^\infty(\mathbf{x}), \quad \forall \mathbf{x} \in S, \end{aligned} \quad (4)$$

for all CNTs ( $S = \cup S_z$ ). This new BIE can be used to solve for the unknown tractions at the interfaces between the CNTs and matrix. For perfect bonding interface conditions (infinitely large stiffness),  $\mathbf{C} = \mathbf{0}$  in Eq. (3), and the above BIE is simplified to

$$\mathbf{u}(\mathbf{x}) = \int_S \mathbf{U}(\mathbf{x}, \mathbf{y})\mathbf{t}(\mathbf{y}) dS(\mathbf{y}) + \mathbf{u}^\infty(\mathbf{x}), \quad \forall \mathbf{x} \in S, \quad (5)$$

which is the BIE used in Ref. [16]. More details in deriving Eq. (5) can be found in Ref. [26].

There are additional unknowns in Eq. (4), that is, the rigid-body motions of each CNT, expressed by Eq. (2) that contains six unknowns ( $\mathbf{d}$  and  $\boldsymbol{\omega}$  vectors) for each CNT. Thus, additional equations are needed to supplement BIE (4). These equations can be obtained by considering equilibrium of each CNT in the form of the following two equations [26]:

$$\int_{S_z} \mathbf{t}(\mathbf{y}) dS(\mathbf{y}) = \mathbf{0} \quad (6)$$

$$\int_{S_z} \mathbf{p}(\mathbf{y}) \times \mathbf{t}(\mathbf{y}) dS(\mathbf{y}) = \mathbf{0} \quad (7)$$

for  $\alpha = 1, 2, \dots, n$ . Eq. (6) represents the equilibrium of the forces, while Eq. (7) that of the moments, for each CNT. BIE (4) and Eqs. (2), (6) and (7) are solved simultaneously to obtain the unknown traction  $\mathbf{t}$ , and rigid-body motions  $\mathbf{d}$  and  $\boldsymbol{\omega}$  for all the CNTs. Once these variables are obtained, integral representations for the displacement and stress fields at any point inside the matrix domain  $V$  can be readily evaluated that can be applied to evaluate the effective elastic properties of the CNT composites [26].

The BEM is employed to discretize and solve the BIE derived above. With the development of the fast multipole methods (a recent review can be found in Ref. [27]) for solving BEM equations, large models with several million DOFs can be solved readily on a desktop computer. The main idea of the fast multipole methods is that elements of integration are grouped into clusters (cells) according to the distance of the elements to the source point. The integrations on elements in one cluster are computed together using multipole expansions. Thus, the number of integrations is reduced and hence the computing time. In addition, with the use of iterative solvers (such as GMRES), the full BEM matrix is never formed explicitly in the fast multipole methods and thus the required memory is also much less for the multipole BEM. Using the fast multipole BEM, the solution time of a problem is reduced to order  $O(N)$ , instead of  $O(N^3)$  as in the traditional BEM with direct solvers (with  $N$  here being the number of equations). In recent years, the fast multipole BEM has also been demonstrated to be especially good for solving problems with large numbers of cracks and inclusions in both 2-D and 3-D cases. Some of the work on solving inclusion problems using the fast multipole BEM can be found in Refs. [28–32]. The details of the FMM BEM formulation and implementation used in this study, including the choice of preconditioners and other parameters used, can be found in Refs. [16,26,27].

### 3. CNT pull-out simulations using MD and the cohesive interface model

To determine the compliance matrix  $\mathbf{C}$  in Eq. (3) or Eq. (4) for the cohesive interface model, detailed molecular dynamics simulations were carried out using models of a CNT with surrounding polymer chains. For load conditions, the CNT is pulled out of the polymer in the axial  $z$ -direction or rotated relative to the polymer in the circumferential  $\theta$ -direction, or the entire model is compressed in the radial  $r$ -direction (Fig. 3). With these three load conditions, the components of the compliance matrix in the local  $(z, r, \theta)$  coordinates can be determined.

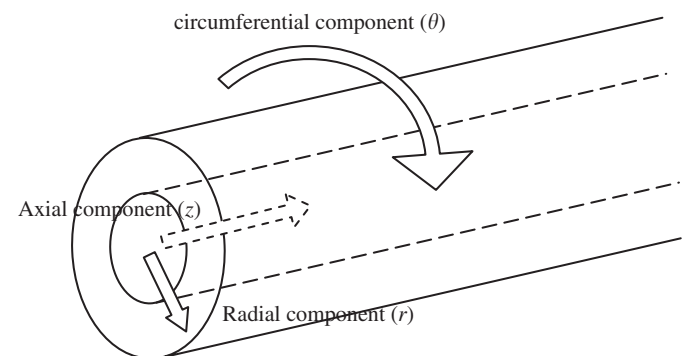


Fig. 3. The local cylindrical coordinates for determining the compliance coefficients.

The models of polyethylene (PE) systems with both amorphous and crystalline polymer chains are used in the molecular dynamics simulations. In both cases, neither cross-link chemical bonds nor coatings are assumed to be present. The CNT is modeled by the Tersoff–Brenner potential [33,34]. The interactions between the CNT and polymer matrix are governed by the Lennard–Jones pair potential with the 6–12 functional dependence. The PE system is modeled by the united atom potential [35], which considers bond stretching, dihedral and torsional effects. In the case of amorphous polymer chains, the CNT chosen is a (10, 0) single-walled CNT, 40 Å long, 3.85 Å radius and with 380 atoms. The system is located in a cell of  $40 \times 40 \times 40 \text{ \AA}^3$  and has 4100–4300 atoms, depending on

the CNT–polymer spacing. The system is simulated using the MD approach. A representative configuration with amorphous polymer chains is shown in Fig. 4(a). A uniform velocity of  $5 \text{ \AA/ps}$  is applied to the boundary atoms of the CNT, so that it pulls out the CNT from the matrix (Fig. 4(b)).

Fig. 5(a) shows the CNT embedded in a crystalline polymer matrix. After the initial configuration is relaxed, the cohesive forces between the CNT and polymer by either pulling it out along the axial direction (Fig. 5(b)), or rotating it with respect to its own axis, are examined. Plotted in Fig. 6(a) and (b) are the cohesive forces per unit length versus the axial displacement and rotation angle, respectively. It is found that the nature of these curves

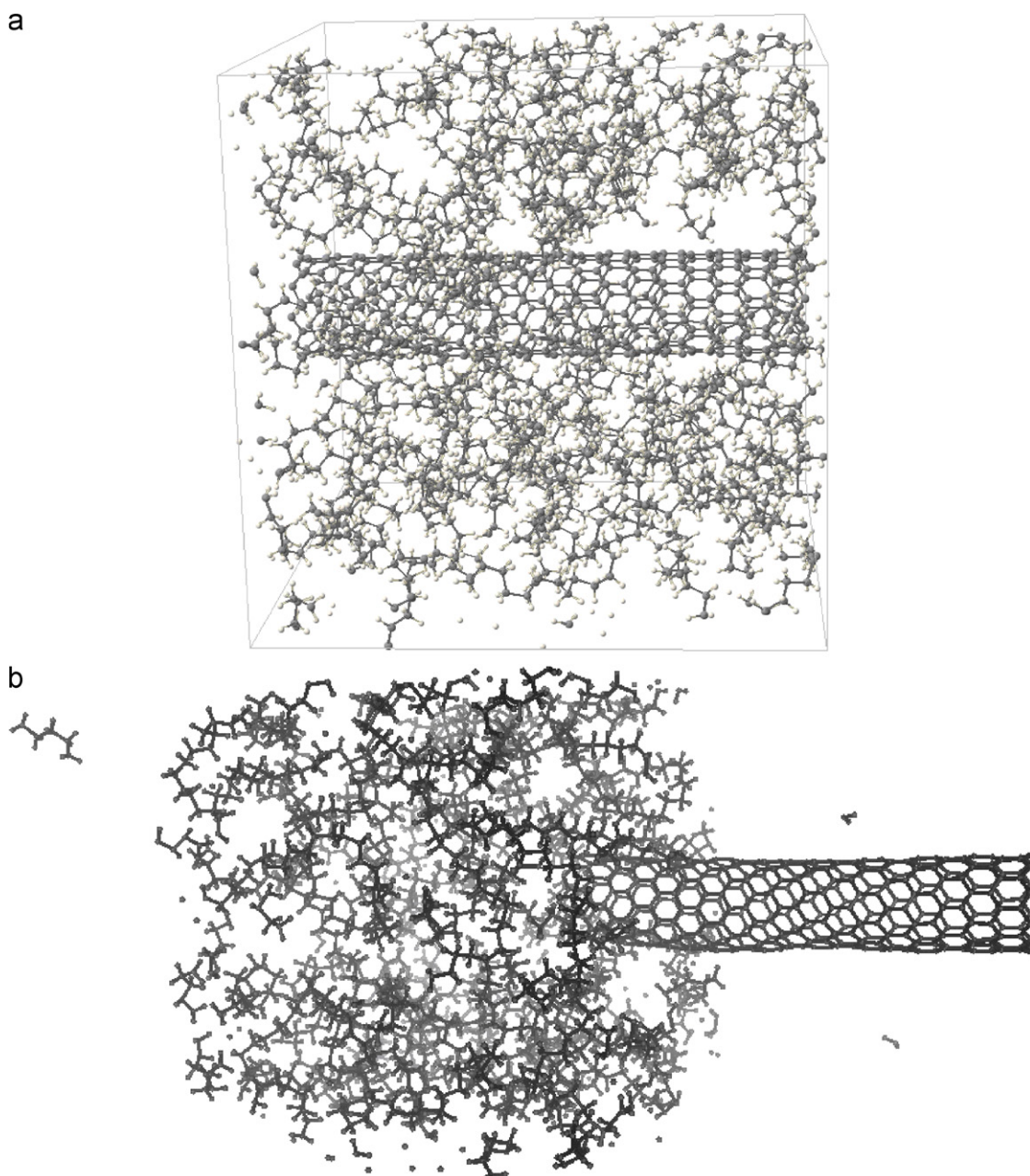


Fig. 4. CNT pull-out test with *amorphous* polymer chains: (a) initial and (b) final configurations of the CNT pull-out test.

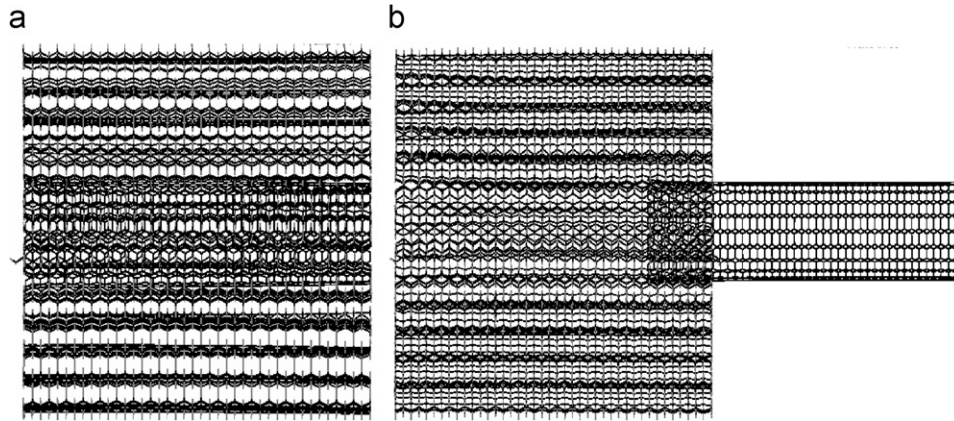


Fig. 5. CNT pull-out test with crystalline polymer chains: (a) initial and (b) final configurations of the CNT pull-out test.

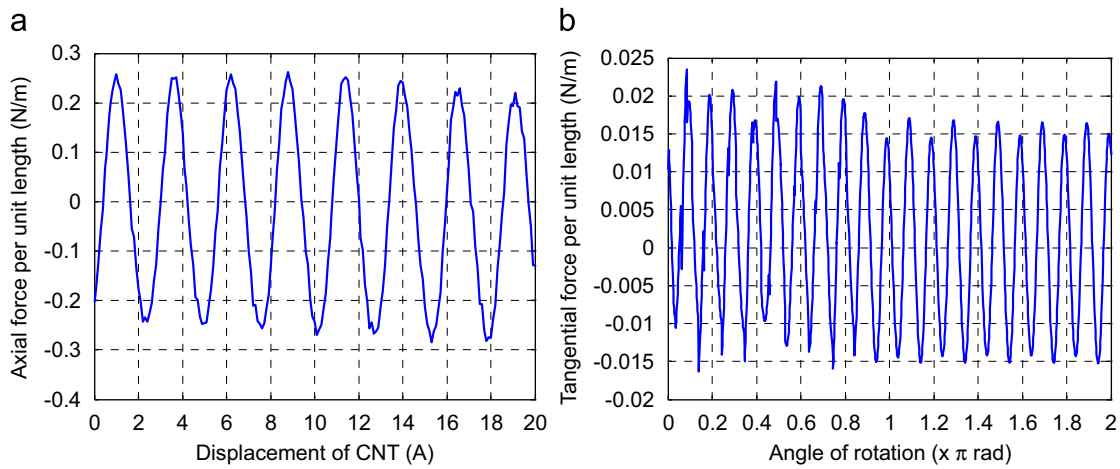


Fig. 6. (a) The axial cohesive force between the CNT and polymer as a function of the displacement and (b) the circumferential cohesive force as a function of the rotation angle [36].

show periodicities that match those of the CNT in the axial and circumferential directions. This indicates that such cohesive force can be well characterized in a form similar to the Mohr–Columb model used in continuum mechanics, although additional considerations of the periodicity are needed. Finally, the variations in the slopes of the cohesive force curves are found to be extremely small which are subsequently used to determine the coefficients in the compliance matrix  $\mathbf{C}$ .

With the molecular simulation results using the above mentioned models for the CNT in crystalline polymer and under the three load conditions, the compliance matrix that relate the traction  $\mathbf{t}$  and displacement  $\mathbf{u}$  at the CNT/polymer interface can be written in the following form:

$$\begin{Bmatrix} \Delta u_z \\ \Delta u_r \\ \Delta u_\theta \end{Bmatrix} = \begin{bmatrix} C_z & 0 & 0 \\ 0 & C_r & 0 \\ 0 & 0 & C_\theta \end{bmatrix} \begin{Bmatrix} t_z \\ t_r \\ t_\theta \end{Bmatrix}, \quad (8)$$

where  $\Delta u$  is the relative displacement of the CNT to the polymer, and the coupling effects (off-diagonal terms in  $\mathbf{C}$ ) are ignored in this preliminary study for simplicity. Details

of the molecular simulations can be found in Refs. [36,37]. The compliance matrix in Eq. (8) will be applied at each node on the interface in the local  $(z, r, \theta)$  coordinates first, and then transformed to the global coordinate system to impose the interface model (Eq. (3)) to the BIE (Eq. (4)).

#### 4. Numerical examples

We first verify the BIE (4) with the cohesive interface model on a problem that has the analytical solution and then show the effect of the cohesive interface model on the effective properties of CNT/polymer composites, as compared with earlier models using the perfect bonding interface model. All the jobs for the numerical examples were run on a FUJITSU PRIMEPOWER HPC2500 supercomputer at the Academic Center of Computing and Media Studies of Kyoto University.

##### 4.1. A rigid sphere embedded in elastic medium with the cohesive interface condition

To validate the BIE for inclusions with cohesive interfaces, we consider a rigid sphere of radius  $a$  in an

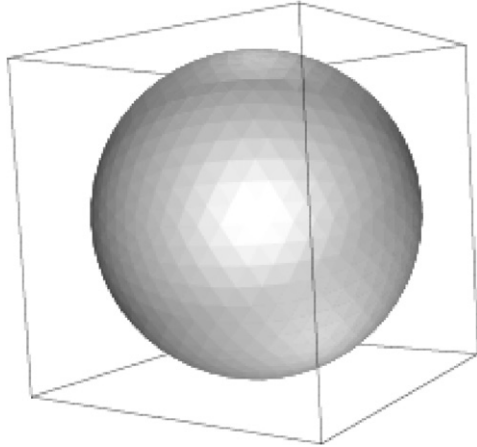


Fig. 7. A rigid sphere in an elastic medium and with cohesive interface conditions.

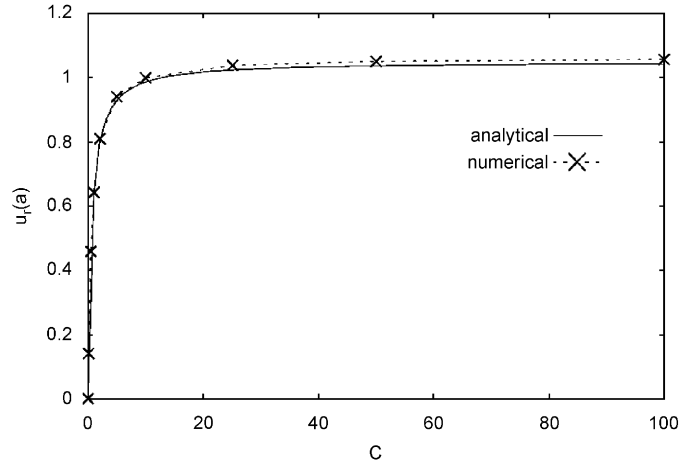


Fig. 8. BEM results for the radial displacement  $u_r(a)$  as a function of  $C$ .

infinite elastic medium (Fig. 7) with Poisson’s ratio  $\nu$ , and Young’s modulus  $E$  (an appropriate non-dimensionalization has been applied). The system is subjected to a remote uniform tri-axial tension  $\sigma^\infty$ . We set  $C_{ij} = C\delta_{ij}$  in the interface condition (3) between the rigid sphere and the elastic medium. The analytical solution for this problem is found to be

$$u_r(r) = \frac{\sigma^\infty}{3\lambda + 2\mu} \left[ 1 - \frac{a - (3\lambda + 2\mu)C a^3}{a + 4\mu C} \frac{a^3}{r^3} \right] r, \quad (9)$$

$$\sigma_r(r) = \frac{\sigma^\infty}{3\lambda + 2\mu} \left[ (3\lambda + 2\mu) + 4\mu \frac{a - (3\lambda + 2\mu)C a^3}{a + 4\mu C} \frac{a^3}{r^3} \right], \quad (10)$$

where  $u_r(r)$  and  $\sigma_r(r)$  are the radial displacement and stress component, respectively; and  $\lambda$  and  $\mu$  are the Lamé constants. The solution in Eqs. (9) and (10) returns to the solution for the perfect bonding case [26] when  $C$  approaches zero, and yields the solution for a void [38] when  $C$  approaches infinity.

Values of the solution in Eqs. (9) and (10) on the interface ( $r=a$ ) are used to verify the BEM solution with various values of the compliance parameter  $C$ . For convenience, we choose  $a=1$  m,  $\sigma^\infty=1$  Pa,  $\nu=0.3$ , and  $E=1$  Pa. The number of boundary elements used on the sphere is 1800. Figs. 8 and 9 show the computed radial displacement and traction on the interface using the BEM and compared with the analytical solution given in Eqs. (9) and (10) for different values of the compliance parameter  $C$ . Very good agreements are obtained as seen in these figures for all values of the compliance parameter  $C$ . Table 1 shows the relative errors in the interface radial displacement values obtained by using the developed BEM. We see that the errors remain less than 1.5% even when  $C$  is large. We also notice that the accuracies for smaller  $C$ s (closer to the perfect bonding interface case) are higher than those for larger  $C$ s (closer to the void case). This example demonstrates that the developed BEM with the cohesive interface model is valid and accurate for analyzing such problems.

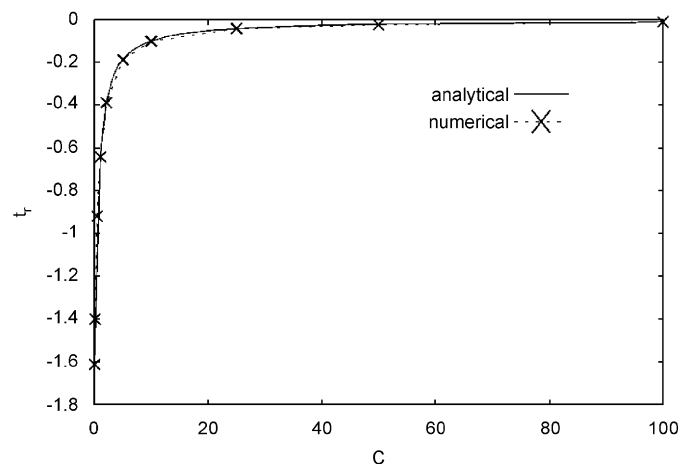


Fig. 9. BEM results for the radial traction  $t_r(a)$  as a function of  $C$ .

Table 1  
Relative errors in the BEM results for the sphere model versus the compliance  $C$

$C$	Error in $u_r(a)$ (%)
0.1	0.11
0.5	0.54
1.0	0.79
5.0	1.20
10.0	1.28
25.0	1.33
50.0	1.35
100.0	1.36

#### 4.2. Effective Young’s moduli of CNT/polymer composites

We use the same BEM models to estimate the effective Young’s moduli of CNT/polymer composites as those in Ref. [16] where perfect bonding interface conditions are used. The length of the CNT fibers considered is 50 nm, the radius of the CNT is 0.7 nm and the CNT thickness is

0.34 nm. The volume of the CNT is calculated by considering it as a hollow cylinder with the outer radius equal to 0.7 nm. For the matrix material, Young's modulus of 1 GPa and Poisson's ratio of 0.4 are used here.

Triangular constant boundary elements are employed in the discretization of the interfaces [16,26]. Each element has 3 degrees of freedom (unknown traction components in this case) and each CNT has additional six unknown rigid-body motions. All the integrals are integrated analytically so that accurate results are ensured even when fibers are packed tightly and surfaces are very close to each other. A boundary element mesh with 600 elements for the CNT fiber is shown in Fig. 10, which yields 1806 degrees of freedom per CNT fiber ( $600 \times 3$  plus 6 unknown rigid-body motions).

The RVEs used to estimate the effective Young's moduli are embedded in the infinite domain filled with the matrix material [16,26]. The CNT fibers are dispersed within the RVEs. In this way, an exterior problem can be solved using

the fast multipole BEM, where boundary elements are only needed at the interfaces of the fibers and the matrix. Some data-collection surfaces are placed coinciding with the surfaces of the RVE (Fig. 11). The displacement and stresses are calculated on these data-collection surfaces. Then, the values of these displacements and stresses are employed to evaluate the effective properties of the composites. More discussions on the RVEs used in this work can be found in Refs. [16,26].

The dimensions of the RVEs studied in this case are  $300 \times 60 \times 60 \text{ nm}^3$ . Arrays of  $5 \times m \times m$  CNT fibers, with  $m$  being the number of CNTs in the  $y$ - and  $z$ -directions, are distributed evenly inside the RVE. However, positions of the CNTs in the  $x$ -direction (CNT axial direction) are "staggered", with a shift equal to half of the CNT length plus the interval between the CNTs in the  $x$ -direction. The number of CNTs in the  $x$ -direction is fixed to 5, while the number of CNTs in the  $y$ - and  $z$ -directions is set to  $m = 2, 4, 5, 6, 8, 10, 11, 12$  to increase the volume fractions of the CNTs in the composites. An RVE with 720 ( $m = 12$ ) CNTs is shown in Fig. 11. A total of  $101 \times 101$  (10,201) internal points are placed evenly on each of the two data-collection surfaces.

From the molecular dynamics simulations of CNT pull-out tests, the axial component in the local  $z$ -direction of the  $\mathbf{C}$  matrix is found to be  $C_z = 3.506$ , and the radial component  $C_r = 0.02157$  (in the non-dimensionalized system). There is a large difference between the values of  $C_z$  and  $C_r$  (more than 160 times). In the present investigation, we set the coefficients of  $\mathbf{C}$  to be  $C_{ij} = C\delta_{ij}$  for simplicity, and carry out computation with various choices of  $C$ . In the determination of the effective moduli, the effect of the axial slip of the CNT is considered important. Therefore, we have to pay attention to the values of  $C_z$  used in the analysis.

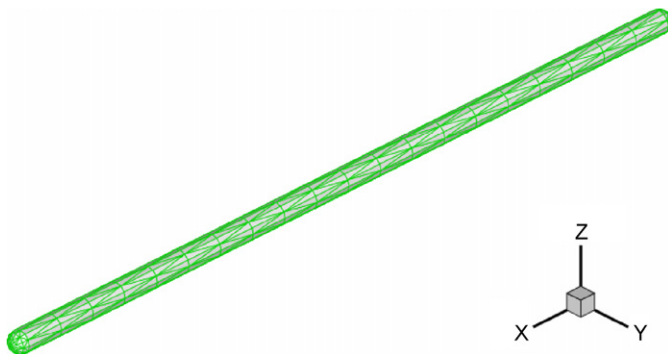


Fig. 10. The boundary element mesh used for modeling the CNT (with 600 elements).

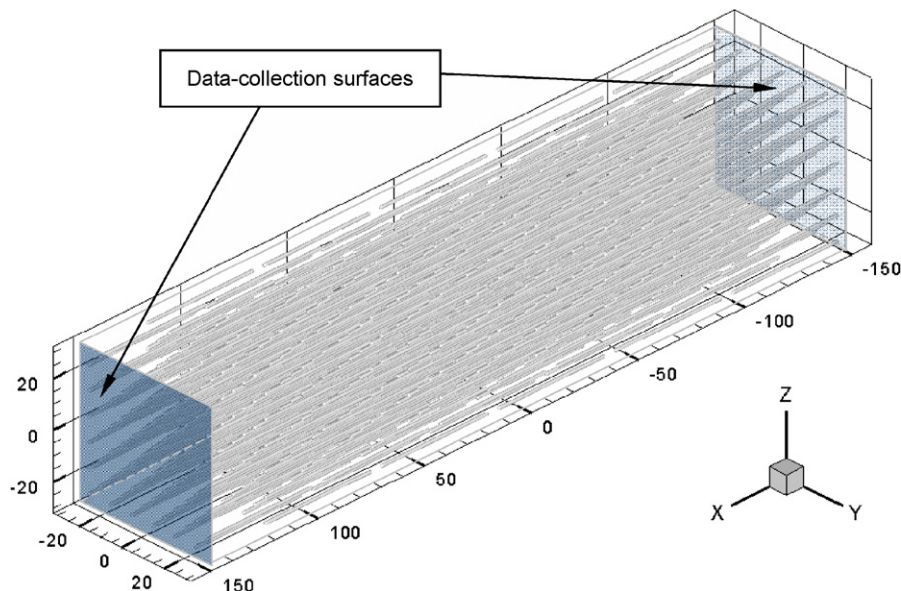


Fig. 11. A BEM model containing 720 CNT fibers.

The following three cases of the interface properties are considered in determining the effective moduli:

- Case 1:  $C = 0$  (no interfacial effects, perfect bonding);
- Case 2:  $C = C_r = 0.02157$  (strong interfacial cohesive force);
- Case 3:  $C = C_z = 3.506$  (weak interfacial cohesive force).

The estimated effective longitudinal Young's moduli ( $E_{eff}$ ) of the CNT composites against the CNT volume fractions are plotted in Fig. 12 for the three cases of  $C$ . Case 1 is based on the perfect bonding interface model used earlier [16], which has been shown to be very close to the results using the MD and continuum mechanics model in Ref. [18] (Fig. 7 in Ref. [18], with CNT length = 50 nm). Case 2 represents a strong interfacial cohesive force case and the estimated effective moduli are very closed to those in Case 1 as shown in Fig. 12. This suggests again that any interface models based on a strong cohesive force model will yield results that are close to those based on perfect bonding interface models. In other words, perfect bonding models would be sufficient if strong interfaces do exist. Case 3 in Fig. 12 represents a weak interface between the CNTs and the matrix, since  $C_z = 3.506$  is the compliance tangent to the interface and in the axial direction of the CNTs. In experiments of CNT composites, slip has been observed in CNT/polymer composite samples [1,19–21]. The estimated effective Young's moduli in Case 3 are indeed much smaller than those in Cases 1 and 2, as expected. About 50% decreases of the values are observed for all the CNT volume fractions. These lower values for the effective moduli are believed to be closer to those in experimental studies (see Ref. [18] for a few limited experimental data points that are lower than the MD simulation results with the strong interface model).

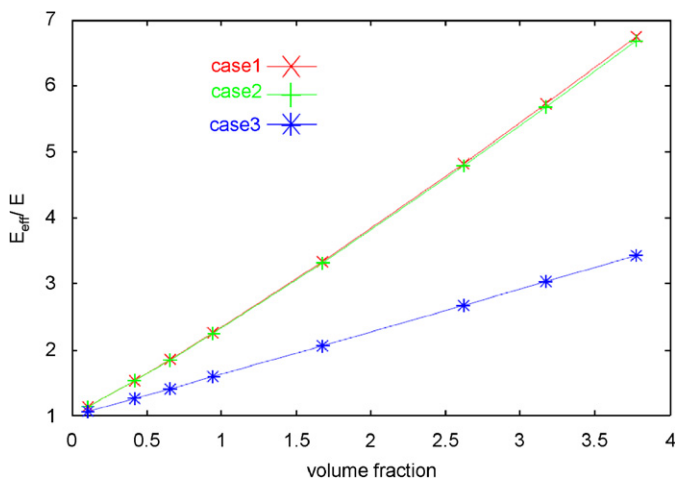


Fig. 12. Effects of the cohesive interface parameter  $C$  on the effective moduli of the composites: Case 1:  $C = 0$  (perfect bonding, the earlier results in Ref. [16]); Case 2:  $C = C_r = 0.02157$  (large interface stiffness); Case 3:  $C = C_z = 3.506$  (small interface stiffness).

However, direct comparisons cannot be made at this time due to the lack of data from the experiments with the same parameters. More studies can be made when the experimental data are available.

## 5. Discussions

The cohesive interface model based on MD simulation results is only the first step in developing multi-scale computational models for such composites. The MD models need to be further investigated and verified against experimental results when they are available. The MD simulation results used to develop the cohesive interface model reported here are preliminary and only meant to establish the procedure to show the feasibility. More MD simulations with different parameters are definitely needed to find the intricate characteristics of the CNT/polymer interfaces and their theoretical models. The interface models should be verified with real physical tests, such as nano-scale CNT pull-out tests. Although these tests are still extremely difficult to perform with the current technologies, these experiments will be very important in validations of the MD simulation results and the developed interface models.

From the BEM results in this paper, it is clear that the interface plays an important role in load transfers and thus the effective properties of the CNT composites. Variations in the interface stiffness can have a significant impact to the results of these estimated properties of the CNT composites. Establishing a valid and effective interface model is a crucial step in the modeling and simulations of the CNT composites. The MD approach employed in this study seems to be a fundamental and effective method for establishing such interface models. The BEM results using the cohesive interface model based on the MD simulations show marked decreases of the effective Young's moduli for the CNT/polymer composites, which are closer to the current experimental observations. More studies are needed, for example, to verify if the cohesive interface model is scale dependent, and to develop other more sophisticated interface models (e.g., with nonlinear properties).

The developed BEM can be extended readily to account for more complicated physics or interactions of the CNT fibers in a composite. Elasticity of the CNTs can be introduced readily in this model to replace the assumption of rigidity for the CNT fibers. Curved CNT fibers, which are often the case in current CNT/polymer composite samples, can also be considered once the rigid-body assumption for the CNT fibers is replaced. An effective-fiber model based on the MD and similar to the one developed in Ref. [18] can also be combined with the BEM models. With the development in computing hardware, it is quite possible in the near future to directly combine the MD model for the CNTs and the BEM model for the matrix to develop a multi-scale method that can handle larger models and account for more intricate physics in

CNT/polymer composites, such as debonding or other failure modes, besides evaluations of their effective properties.

## 6. Conclusion

A new boundary element method using a cohesive interface model for modeling the CNT/polymer composites is presented in this paper. The CNTs are treated as rigid fibers due to their exceptionally high stiffness compared with many polymer matrices. A cohesive interface model is proposed based on molecular dynamics simulations. The estimated effective Young's moduli using this cohesive interface model and the BEM are found to be very close to those reported earlier for strong interface cases and show marked decreases for weak interface cases. These results clearly demonstrate the usefulness, efficiency and promises of the developed BEM as a fast numerical tool for large-scale characterizations of the CNT/polymer composites. For future work, elasticity of the CNT fibers can be considered readily in this BEM and a multi-scale approach solving the MD and the BEM equations simultaneously can also be developed.

## Acknowledgments

The first author (Y.J.L) would like to acknowledge the support of the Japan Society for the Promotion of Science (JSPS) fellowship, the Academic Center for Computing and Media Studies of Kyoto University, and the Chunhui fellowship of the Ministry of Education of China.

## References

- [1] Thostenson ET, Ren ZF, Chou T-W. Advances in the science and technology of carbon nanotubes and their composites: a review. *Compos Sci Technol* 2001;61:1899–912.
- [2] Qian D, Wagner GJ, Liu WK, Yu M-F, Ruoff RS. Mechanics of carbon nanotubes. *Appl Mech Rev* 2002;55:495–533.
- [3] Ruoff RS, Lorents DC. Mechanical and thermal properties of carbon nanotubes. *Carbon* 1995;33:925–30.
- [4] Treacy MMJ, Ebbesen TW, Gibson JM. Exceptionally high Young's modulus observed for individual carbon nanotubes. *Nature* 1996;381:678–80.
- [5] Wong EW, Sheehan PE, Lieber CM. Nanobeam mechanics: elasticity, strength, and toughness of nanorods and nanotubes. *Science* 1997;277:1971–5.
- [6] Lu JP. Elastic properties of single and multilayered nanotubes. *J Phys Chem Solids* 1997;58:1649–52.
- [7] Lu JP. Elastic properties of carbon nanotubes and nanoropes. *Phys Rev Lett* 1997;79:1297–300.
- [8] Buongiorno Nardelli M, Fattbert J-L, Orlikowski D, Roland C, Zhao Q, Bernholc J. Mechanical properties, defects and electronic behavior of carbon nanotubes. *Carbon* 2000;38:1703–11.
- [9] Li C, Chou T-W. Elastic moduli of multi-walled carbon nanotubes and the effect of van der Waals forces. *Compos Sci Technol* 2003;63:1517–24.
- [10] Griebel M, Hamaekers J. Molecular dynamics simulations of the elastic moduli of polymer-carbon nanotube composites. *Comput Methods Appl Mech Eng* 2004;193:1773–88.
- [11] Fisher FT, Bradshaw RD, Brinson LC. Effects of nanotube waviness on the modulus of nanotube-reinforced polymers. *Appl Phys Lett* 2002;80:4647–9.
- [12] Fisher FT, Bradshaw RD, Brinson LC. Fiber waviness in nanotube-reinforced polymer composites—I. Modulus predictions using effective nanotube properties. *Compos Sci Technol* 2003;63:1689–703.
- [13] Liu YJ, Chen XL. Continuum models of carbon nanotube-based composites using the boundary element method. *Electron J Boundary Elem* 2003;1:316–35.
- [14] Liu YJ, Chen XL. Evaluations of the effective materials properties of carbon nanotube-based composites using a nanoscale representative volume element. *Mech Mater* 2003;35:69–81.
- [15] Chen XL, Liu YJ. Square representative volume elements for evaluating the effective material properties of carbon nanotube-based composites. *Comput Mater Sci* 2004;29:1–11.
- [16] Liu YJ, Nishimura N, Otani Y. Large-scale modeling of carbon-nanotube composites by the boundary element method based on a rigid-inclusion model. *Comput Mater Sci* 2005;34:173–87.
- [17] Odegard GM, Gates TS, Nicholson LM, Wise KE. Equivalent-continuum modeling of nano-structured materials. *Compos Sci Technol* 2002;62:1869–80.
- [18] Odegard GM, Gates TS, Wise KE, Park C, Siochi EJ. Constitutive modeling of nanotube-reinforced polymer composites. *Compos Sci Technol* 2003;63:1671–87.
- [19] Schadler LS, Giannaris SC, Ajayan PM. Load transfer in carbon nanotube epoxy composites. *Appl Phys Lett* 1998;73:3842–4.
- [20] Qian D, Dickey EC, Andrews R, Rantell T. Load transfer and deformation mechanisms in carbon nanotube-polystyrene composites. *Appl Phys Lett* 2000;76:2868–70.
- [21] Ajayan PM, Schadler LS, Giannaris C, Rubio A. Single-walled carbon nanotube-polymer composites: strength and weakness. *Adv Mater* 2000;12:750–3.
- [22] Odegard GM, Pipes RB, Hubert P. Comparison of two models of SWCN polymer composites. *Compos Sci Technol* 2004;64:1011–20.
- [23] Mukherjee S. Boundary element methods in creep and fracture. New York: Applied Science Publishers; 1982.
- [24] Banerjee PK. The boundary element methods in engineering. 2nd ed. New York: McGraw-Hill; 1994.
- [25] Brebbia CA, Dominguez J. Boundary elements—an introductory course. New York: McGraw-Hill; 1989.
- [26] Liu YJ, Nishimura N, Otani Y, Takahashi T, Chen XL, Munakata H. A fast boundary element method for the analysis of fiber-reinforced composites based on a rigid-inclusion model. *J Appl Mech* 2005;72:115–28.
- [27] Nishimura N. Fast multipole accelerated boundary integral equation methods. *Appl Mech Rev* 2002;55:299–324.
- [28] Greengard LF, Helsing J. On the numerical evaluation of elastostatic fields in locally isotropic two-dimensional composites. *J Mech Phys Solids* 1998;46:1441–62.
- [29] Greengard LF, Kropinski MC, Mayo A. Integral equation methods for Stokes flow and isotropic elasticity in the plane. *J Comput Phys* 1996;125:403–14.
- [30] Helsing J. An integral equation method for elastostatics of periodic composites. *J Mech Phys Solids* 1995;43:815–28.
- [31] Greengard LF, Rokhlin V. A fast algorithm for particle simulations. *J Comput Phys* 1987;73:325–48.
- [32] Fu Y, Klimkowski KJ, Rodin GJ, Berger E, Browne JC, Singer JK, et al. A fast solution method for three-dimensional many-particle problems of linear elasticity. *Int J Numer Methods Eng* 1998;42:1215–29.
- [33] Brenner DW. Empirical potential for hydrocarbons for use in simulating the chemical vapor-deposition of diamond films. *Phys Rev B* 1990;42:9458–71.
- [34] Tersoff J. Empirical interatomic potential for carbon, with applications to amorphous-carbon. *Phys Rev Lett* 1988;61:2879–82.

- [35] Mokashi V, Qian D. A software package based on modifications made to the DL\_POLY package. <[http://www.cse.clrc.ac.uk/msi/software/DL\\_POLY](http://www.cse.clrc.ac.uk/msi/software/DL_POLY)>, 2004.
- [36] Mokashi V. Study of mechanical properties of carbon nanotubes and nanocomposites by molecular simulations, Master Thesis, 2005, University of Cincinnati.
- [37] Mokashi V, Qian D, Liu YJ. A study on the tensile response and fracture in carbon nanotube-based composites using molecular mechanics. *Compos Sci Technol* 2007;67(3–4):530–40.
- [38] Timoshenko SP, Goodier JN. *Theory of elasticity*. 3rd ed. New York: McGraw-Hill; 1987.